
Self-Adaptive Physics-Informed Neural Networks using a Soft Attention Mechanism

Levi D. McClenney* Ulisses Braga-Neto

Department of Electrical and Computer Engineering
 Texas A&M University
 College Station, TX USA
 {levimcclenny,ulisses}@tamu.edu

Abstract

Physics-Informed Neural Networks (PINNs) have emerged recently as a promising application of deep neural networks to the numerical solution of nonlinear partial differential equations (PDEs). However, the original PINN algorithm is known to suffer from stability and accuracy problems in cases where the solution has sharp spatio-temporal transitions. These “stiff” PDEs require an unreasonably large number of collocation points to be solved accurately. It has been recognized that adaptive procedures are needed to force the neural network to fit accurately the stubborn spots in the solution of stiff PDEs. To accomplish this, previous approaches have used fixed weights hard-coded over regions of the solution deemed to be important. In this paper, we propose a fundamentally new method to train PINNs adaptively, where the adaptation weights are fully trainable, so the neural network learns by itself which regions of the solution are difficult and is forced to focus on them, which is reminiscent of soft multiplicative-mask attention mechanism used in computer vision. The basic idea behind these Self-Adaptive PINNs is to make the weights increase where the corresponding loss is higher, which is accomplished by training the network to simultaneously minimize the losses and maximize the weights, i.e., to find a saddle point in the cost surface. We show that this is formally equivalent to solving a PDE-constrained optimization problem using a penalty-based method, though in a way where the monotonically-nondecreasing penalty coefficients are trainable. Numerical experiments with an Allen-Cahn “stiff” PDE, the Self-Adaptive PINN outperformed other state-of-the-art PINN algorithms in L2 error by a wide margin, while using a smaller number of training epochs. An Appendix contains additional results with Burger’s and Helmholtz PDEs, which confirmed the trends observed in the Allen-Cahn experiments.

1 Introduction

As part of the burgeoning field of scientific machine learning [1], physics-informed neural networks (PINNs) have emerged recently as an alternative to traditional partial differential equation (PDE) solvers [2, 3, 4, 5]. Typical black-box deep learning methodologies do not take into account physical understanding of the problem domain. The PINN approach is based on constraining the output of a deep neural network to satisfy a physical model specified by a PDE. The potential of using neural networks as universal function approximators to solve PDEs had been recognized since the 1990’s [6]. However, PINNs promise to take this approach to a different level by using deep neural networks, which is made possible by the vast advances in computational capabilities and training algorithms since that time [7, 8], as well as by the invention of automatic differentiation methods [9, 10].

*levimcclenny@tamu.edu, levimcclenny.com

A great advantage of PINNs over traditional time-stepping PDE solvers is that the entire spatial-temporal domain can be solved at once using collocation points distributed irregularly (rather than on a grid) across the spatial-temporal domain, in a process that can be massively parallelized via GPU. As we have continued to see GPU capabilities increase in recent years, a method that relies on parallelism in training iterations will likely emerge as the predominant approach in scientific computing.

The original continuous PINN algorithm proposed in [2], henceforth referred to as the “baseline PINN” algorithm, is effective at estimating solutions that are reasonably smooth, such as Burgher’s equation, the wave equation, Poisson’s equation, and Schrodinger’s equation. On the other hand, it has been observed that the baseline PINN has convergence and accuracy problems when solving “stiff” PDEs [11] with solutions that contain sharp and intricate space and time transitions [4, 12]. This is the case, for example, of the Allen-Cahn and Cahn-Hilliard equations of phase-field models [13].

To address this issue, various modifications of the baseline PINN algorithm have been proposed. For example, in [4], a series of schemes are introduced, including nonadaptive weighting of the training loss function, adaptive resampling of the collocation points, and time-adaptive approaches, while in [12], a learning rate annealing scheme was proposed. The consensus has been that adaptation mechanisms are essential to make PINNs more stable and able to approximate well difficult regions of the solution.

This paper introduces Self-Adaptive PINNs, a fundamentally new method to train PINNs adaptively, which uses trainable weights as a soft multiplicative mask reminiscent of the attention mechanism used in computer vision [14, 15]. The adaptation weights are trained concurrently with the network weights. As a result, initial, boundary or collocation points in difficult regions of the solution are automatically weighted more in the loss function, forcing the approximation to improve on those points. The basic principle in Self-Adaptive PINNs is to make the weights increase where the corresponding losses are higher, which is accomplished by training the network to simultaneously minimize the losses and maximize the weights, i.e., to find a saddle point in the cost surface. We show that this is formally equivalent to a penalty-based solution of PDE-constrained optimization methods. Experimental results show that Self-Adaptive PINNs can solve a “stiff” Allen-Cahn PDE with significantly better accuracy than other state-of-the-art PINN algorithms, while using a smaller number of training epochs. We also report in the Appendix results obtained with easier-to-solve Burger’s and Helmholtz PDEs, which confirm the trends observed in the Allen-Cahn experiments.

2 Background

2.1 Overview of Physics-Informed Neural Networks

Consider a general nonlinear PDE of the form:

$$\mathcal{N}_{\mathbf{x},t}[u(\mathbf{x}, t)] = 0, \quad \mathbf{x} \in \Omega, \quad t \in [0, T], \quad (1)$$

$$u(\mathbf{x}, t) = g(\mathbf{x}, t), \quad \mathbf{x} \in \partial\Omega, \quad t \in [0, T], \quad (2)$$

$$u(\mathbf{x}, 0) = h(\mathbf{x}), \quad \mathbf{x} \in \Omega, \quad (3)$$

where $\mathbf{x} \in \Omega$ is a spatial vector variable in a domain $\Omega \subset \mathbb{R}^d$, t is time, and $\mathcal{N}_{\mathbf{x},t}$ is a spatial-temporal differential operator. Following [2], let $u(\mathbf{x}, t)$ be approximated by the output $u_{\theta}(\mathbf{x}, t)$ of a deep neural network with inputs \mathbf{x} and t . Define the approximation network $u(\mathbf{x}, t; \mathbf{w})$ and the residual network $r(\mathbf{x}, t; \mathbf{w})$, which share the same network weights \mathbf{w} and satisfy:

$$r(\mathbf{x}, t; \mathbf{w}) := \mathcal{N}_{\mathbf{x},t}[u(\mathbf{x}, t; \mathbf{w})], \quad (4)$$

where all partial derivatives can be computed by automatic differentiation methods [9, 10]. The shared network weights \mathbf{w} are trained by minimizing a loss function that penalizes the output for not satisfying (1)-(3):

$$\mathcal{L}(\mathbf{w}) = \mathcal{L}_s(\mathbf{w}) + \mathcal{L}_r(\mathbf{w}) + \mathcal{L}_b(\mathbf{w}) + \mathcal{L}_0(\mathbf{w}), \quad (5)$$

where \mathcal{L}_s is the loss corresponding to sample data (if any), \mathcal{L}_r is the loss corresponding to the residual (4), \mathcal{L}_b is the loss due to the boundary conditions (2), and \mathcal{L}_0 is the loss due to the initial

conditions (3):

$$\mathcal{L}_s(\mathbf{w}) = \frac{1}{N_s} \sum_{i=1}^{N_s} |u(\mathbf{x}_s^i, t_s^i; \mathbf{w}) - y_s^i|^2, \quad (6)$$

$$\mathcal{L}_r(\mathbf{w}) = \frac{1}{N_r} \sum_{i=1}^{N_r} r(\mathbf{x}_r^i, t_r^i; \mathbf{w})^2, \quad (7)$$

$$\mathcal{L}_b(\mathbf{w}) = \frac{1}{N_b} \sum_{i=1}^{N_b} |u(\mathbf{x}_b^i, t_b^i; \mathbf{w}) - g_b^i|^2, \quad (8)$$

$$\mathcal{L}_0(\mathbf{w}) = \frac{1}{N_0} \sum_{i=1}^{N_0} |u(\mathbf{x}_0^i, 0; \mathbf{w}) - h_0^i|^2, \quad (9)$$

where $\{\mathbf{x}_s^i, t_s^i, y_s^i\}_{i=1}^{N_s}$ are sample data (if any), $\{\mathbf{x}_0^i, h_0^i = h(\mathbf{x}_0^i)\}_{i=1}^{N_0}$ are initial condition point, $\{\mathbf{x}_b^i, t_b^i, g_b^i = g(\mathbf{x}_b^i, t_b^i)\}_{i=1}^{N_b}$ are boundary condition points, $\{\mathbf{x}_r^i, t_r^i\}_{i=1}^{N_r}$ are collocation points randomly distributed in the domain Ω , and N_s, N_0, N_b and N_r denote the total number of sample data, initial points, boundary points, and collocation points, respectively. The network weights \mathbf{w} can be tuned by minimizing the total training loss $\mathcal{L}(\mathbf{w})$ via standard gradient descent procedures used in deep learning.

2.2 Related Work

The baseline PINN algorithm can be unstable during training and produce inaccurate approximations around sharp space and time transitions in the solution of “stiff” PDEs. Much of the recent literature on PINNs has been devoted to mitigating these issues by introducing modifications to the baseline PINN algorithm that can increase training stability and accuracy of the approximation. We mention some of these approaches below.

Nonadaptive Weighting. In [4], it was pointed out that a premium should be put on forcing the neural network to satisfy the initial conditions closely, especially for PDEs describing time-irreversible processes, where the solution has to be approximated well early. Accordingly, a loss function of the form $\mathcal{L}(\theta) = \mathcal{L}_r(\theta) + \mathcal{L}_b(\theta) + C \mathcal{L}_0(\theta)$ was suggested, where $C \gg 1$ is a hyperparameter.

Learning Rate Annealing. In [12], it is argued that the optimal value of the weight C in the previous scheme may vary wildly among different PDEs so that choosing its value would be difficult. Instead they propose to use weights that are tuned during training using statistics of the backpropagated gradients of the loss function. It is noteworthy that the weights themselves are not adjusted by backpropagation. Instead, they behave as learning rate coefficients, which are updated after each epoch of training.

Adaptive Resampling. In [4], a strategy to adaptively resample the residual collocation points based on the magnitude of the residual is proposed. While this approach improves the approximation, the training process must be interrupted and the MSE evaluated on the residual points to deterministically resample the ones with the highest error. After each resampling step, the number of residual points grows, increasing computational complexity.

Stochastic Gradient Descent. A training procedure where a different subset of collocation points are randomly sampled at each iteration was proposed by [12]. While stochastic gradient descent approaches a global minimum in an infinite limit [16], it is a random method that relies on sufficient random sampling and a large training horizon, which may be computationally intractable.

Time-Adaptive Approaches. In [4], another method is suggested, which divides the time axis into several smaller intervals, and trains PINNs separately on them, either sequentially or in parallel. This approach is time-consuming due to the need to train multiple PINNs.

Neural Tangent Kernel (NTK) Weighting. Most recently, [5] introduced weights on the collocation and boundary losses, which are updated via neural tangent kernels. This approach derives a deterministic kernel which remains constant during training.

3 Methods

While the methods outlined in the previous section produce improvements in stability and accuracy over the baseline PINN, they are either nonadaptive or require brute-force adaptation at increased computational cost. Here we propose a simple procedure that uses fully-trainable weights and require no extra hyperparameters. Instead of hard-coding weights at particular regions of the solution, it is in agreement with the neural network philosophy of self-adaptation, where the adaptation weights in the loss function are updated by backpropagation together with the network weights. In effect, the adaptation weights behave as a multiplicative soft attention mask, in a way that is reminiscent of attention mechanisms used in computer vision [14, 15].

Self-adaptive PINN utilizes the following loss function

$$\mathcal{L}(\mathbf{w}, \boldsymbol{\lambda}_r, \boldsymbol{\lambda}_b, \boldsymbol{\lambda}_0) = \mathcal{L}_s(\mathbf{w}) + \mathcal{L}_r(\mathbf{w}, \boldsymbol{\lambda}_r) + \mathcal{L}_b(\mathbf{w}, \boldsymbol{\lambda}_b) + \mathcal{L}_0(\mathbf{w}, \boldsymbol{\lambda}_0), \quad (10)$$

where $\boldsymbol{\lambda}_r = (\lambda_r^1, \dots, \lambda_r^{N_r})$, $\boldsymbol{\lambda}_b = (\lambda_b^1, \dots, \lambda_b^{N_b})$, and $\boldsymbol{\lambda}_0 = (\lambda_0^1, \dots, \lambda_0^{N_0})$ are trainable *self-adaptation weights* for the initial, boundary, and collocation points, respectively, and

$$\mathcal{L}_r(\mathbf{w}, \boldsymbol{\lambda}_r) = \frac{1}{N_r} \sum_{i=1}^{N_r} [\lambda_r^i r(\mathbf{x}_r^i, t_r^i; \mathbf{w})]^2 \quad (11)$$

$$\mathcal{L}_b(\mathbf{w}, \boldsymbol{\lambda}_b) = \frac{1}{N_b} \sum_{i=1}^{N_b} [\lambda_b^i (u(\mathbf{x}_b^i, t_b^i; \mathbf{w}) - g_b^i)]^2 \quad (12)$$

$$\mathcal{L}_0(\mathbf{w}, \boldsymbol{\lambda}_0) = \frac{1}{N_0} \sum_{i=1}^{N_0} [\lambda_0^i (u(\mathbf{x}_0^i, 0; \mathbf{w}) - h_0^i)]^2. \quad (13)$$

The trainable weights force the network to fit as closely as possible the initial, boundary, or residual points. The sample data loss is not weighted, as these data consist of noisy observations, and forcing the network to fit them closely might contribute to overfitting.

The key feature of self-adaptive PINNs is that the loss $\mathcal{L}(\mathbf{w}, \boldsymbol{\lambda}_r, \boldsymbol{\lambda}_b, \boldsymbol{\lambda}_0)$ is minimized with respect to the network weights \mathbf{w} , as usual, but is *maximized* with respect to the self-adaptation weights $\boldsymbol{\lambda}_r, \boldsymbol{\lambda}_b, \boldsymbol{\lambda}_0$; in other words, training seeks a saddle point

$$\min_{\mathbf{w}} \max_{\boldsymbol{\lambda}_r, \boldsymbol{\lambda}_b, \boldsymbol{\lambda}_0} \mathcal{L}(\mathbf{w}, \boldsymbol{\lambda}_r, \boldsymbol{\lambda}_b, \boldsymbol{\lambda}_0). \quad (14)$$

This can be accomplished by a gradient descent/ascent procedure, with updates given by:

$$\mathbf{w}^{k+1} = \mathbf{w}^k - \eta_k \nabla_{\mathbf{w}} \mathcal{L}(\mathbf{w}^k, \boldsymbol{\lambda}_r^k, \boldsymbol{\lambda}_b^k, \boldsymbol{\lambda}_0^k) \quad (15)$$

$$\boldsymbol{\lambda}_r^{k+1} = \boldsymbol{\lambda}_r^k + \eta_k \nabla_{\boldsymbol{\lambda}_r} \mathcal{L}(\mathbf{w}^k, \boldsymbol{\lambda}_r^k, \boldsymbol{\lambda}_b^k, \boldsymbol{\lambda}_0^k) \quad (16)$$

$$\boldsymbol{\lambda}_b^{k+1} = \boldsymbol{\lambda}_b^k + \eta_k \nabla_{\boldsymbol{\lambda}_b} \mathcal{L}(\mathbf{w}^k, \boldsymbol{\lambda}_r^k, \boldsymbol{\lambda}_b^k, \boldsymbol{\lambda}_0^k) \quad (17)$$

$$\boldsymbol{\lambda}_0^{k+1} = \boldsymbol{\lambda}_0^k + \eta_k \nabla_{\boldsymbol{\lambda}_0} \mathcal{L}(\mathbf{w}^k, \boldsymbol{\lambda}_r^k, \boldsymbol{\lambda}_b^k, \boldsymbol{\lambda}_0^k). \quad (18)$$

where η_k is the learning rate at step k . Considering the self-adaptation weights $\boldsymbol{\lambda}_0$, to fix ideas, we see that

$$\nabla_{\boldsymbol{\lambda}_0} \mathcal{L}(\mathbf{w}^k, \boldsymbol{\lambda}_r^k, \boldsymbol{\lambda}_b^k, \boldsymbol{\lambda}_0^k) = 2 \left(\lambda_0^{k,1} (u(\mathbf{x}_0^1, 0) - h_0^1)^2, \dots, \lambda_0^{k,N_0} (u(\mathbf{x}_0^{N_0}, 0) - h_0^{N_0})^2 \right) \geq 0, \quad (19)$$

provided that $\boldsymbol{\lambda}_0^k \geq 0$. This shows that the sequence of weights $\{\boldsymbol{\lambda}_0^k; k = 1, 2, \dots\}$ is monotonically nondecreasing, provided that $\boldsymbol{\lambda}_0^1$ is initialized to a nonnegative value. Furthermore, (19) shows that the magnitude of the gradient, and therefore of the update, is larger when the errors $(u(\mathbf{x}_0^i, 0) - h_0^i)^2$ and the weights $\lambda^{k,i}$ themselves are large. This progressively penalizes the network more for not fitting the initial boundary points closely. These facts are true for all self-adaptation weights. Notice that any of the weights can be set to fixed, non-trainable values, if desired. For example, by setting $\lambda_b^k \equiv 1$, only the weights of the initial and collocation points would be trained.

For another perspective, consider the PDE-constrained optimization problem

$$\min \sum_{i=1}^{N_s} |u(\mathbf{x}_s^i, t_s^i; \mathbf{w}) - y_s^i|^2 \quad (20)$$

subject to

$$\mathcal{N}_{\mathbf{x}, t}[u(\mathbf{x}, t; \mathbf{w})] = 0, \quad i = 1, \dots, N_r \quad (21)$$

$$u(\mathbf{x}_b^i, t_b^i; \mathbf{w}) = g_b^i, \quad i = 1, \dots, N_b \quad (22)$$

$$u(\mathbf{x}_0^i, t_0^i; \mathbf{w}) = h_0^i, \quad i = 1, \dots, N_0 \quad (23)$$

$$(24)$$

Formally, Self-Adaptive PINN training corresponds to a *penalty method* to solve this PDE-constrained optimization problem [17]. In a typical penalty optimization method, a constrained problem

$$\min f(\mathbf{x}) \quad (25)$$

subject to

$$h(\mathbf{x}) = 0 \quad (26)$$

is solved as a sequence of unconstrained problems

$$\min f(\mathbf{x}) + c^k P(\mathbf{x}), \quad k = 1, 2, \dots, \quad (27)$$

where $c^1 < c^2 < \dots$ is a fixed sequence of increasing penalty costs, and $P(\mathbf{x})$ is a suitable *penalty function*, which is small in the feasible region, and large outside of it. A typical choice is $P(\mathbf{x}) = |h(\mathbf{x})|^p$, for $p > 1$. It can be shown that a limit point of a sequence of solutions of the unconstrained problem, where the solution at step k is used as the initialization for step $k + 1$, is a solution of the original constrained problem [17].

One can see that Self-Adaptive PINN training is a penalty method, where $P(\mathbf{x}) = |h(\mathbf{x})|^2$ and the costs $c^k = \lambda^k$ are the self-adaptation weights during training. Though the self-adaptation weights still form a nondecreasing sequence, they are not selected a-priori, but are adaptively updated by the neural network training procedure. We remark that the use of neural networks to solve penalty-based constrained optimization problems has been proposed previously [18, 19] but not using trainable weights, as far as we know.

The gradient ascent/descent step can be implemented easily using off-the-self neural network software, by simply flipping the sign of $\nabla_{\lambda_r} \mathcal{L}$, $\nabla_{\lambda_b} \mathcal{L}$, and $\nabla_{\lambda_0} \mathcal{L}$. In our implementation of Self-Adaptive PINNs, we use Tensorflow with a fixed number of iterations of Adam [20] followed by another fixed number of iterations of the L-BFGS quasi-newton method [21]. This is consistent with the baseline PINN formulation in [2], as well as follow-up literature [4]. However, the adaptive weights are only updated in the Adam training steps, and are held constant during L-BFGS training. A full implementation of the methodology described here has been made publicly available by the authors².

4 Results

In this section, we report experimental results obtained with the Allen-Cahn PDE, which contrast the performance of the proposed Self-Adaptive PINN algorithm against the baseline PINN and two of the PINN algorithms mentioned in Section 2.2, namely, the nonadaptive weighting and time-adaptive schemes (for the latter, Approach 1 in [4] was used).

The main figure of merit used is the L2-error:

$$L_2 \text{ error} = \frac{\sqrt{\sum_{i=1}^{N_U} |u(x_i, t_i) - U(x_i, t_i)|^2}}{\sqrt{\sum_{i=1}^{N_U} |U(x_i, t_i)|^2}}. \quad (28)$$

where $u(x, t)$ is the trained approximation, and $U(x, t)$ is a high-fidelity solution over a mesh $\{x_i, t_i\}$ containing N_U points. We repeat the training process over a number of random restarts and report the average L2 error and its standard deviation.

²<https://github.com/levimcclelly/SA-PINNs>

4.1 Allen-Cahn Equation

The Allen-Cahn reaction-diffusion PDE is typically encountered in phase-field models, which can be used, for instance, to simulate the phase separation process in the microstructure evolution of metallic alloys [13, 22, 23]. The Allen-Cahn PDE considered here is specified as follows:

$$u_t - 0.0001u_{xx} + 5u^3 - 5u = 0, \quad x \in [-1, 1], \quad t \in [0, 1], \quad (29)$$

$$u(x, 0) = x^2 \cos(\pi x), \quad (30)$$

$$u(t, -1) = u(t, 1), \quad (31)$$

$$u_x(t, -1) = u_x(t, 1), \quad (32)$$

The Allen-Cahn PDE is an interesting benchmark for PINNs for multiple reasons. It is a “stiff” PDE that challenges PINNs to approximate solutions with sharp space and time transitions, and is also introduces periodic boundary conditions (31, 32). In order to deal with the latter, the boundary loss function $\mathcal{L}_b(\theta, \mathbf{w}_b)$ in (12) is replaced by

$$\mathcal{L}_b(\mathbf{w}, \boldsymbol{\lambda}_b) = \frac{1}{N_b} \sum_{i=1}^{N_b} |\lambda_b^i|^2 (|u(1, t_b^i) - u(-1, t_b^i)|^2 + |u_x(1, t_b^i) - u_x(-1, t_b^i)|^2) \quad (33)$$

The neural network architecture is fully connected with layer sizes [2, 128, 128, 128, 128, 1]. (The 2 inputs to the network are (x, t) pairs and the output is the approximated value of u_θ .) This architecture is identical to [4], in order to allow a direct comparison of performance. We set the number of collocation, initial, and boundary points to $N_r = 20,000$, $N_0 = 100$ and $N_b = 100$, respectively (due to the periodic boundary condition, there are in fact 200 boundary points). Here we hold the boundary weights w_b^i at 1, while the initial weights w_0^i and collocation weights w_r^i are trained. The initial and collocation weights are initialized from a uniform distribution in the intervals $[0, 100]$ and $[0, 1]$, respectively. Training took 65ms/iteration on a single Nvidia V100 GPU.

Numerical results obtained with the Self-Adaptive PINN are displayed in figure 1. The average L2 error across 10 runs with random restarts was $2.1\% \pm 1.21\%$, while the L2 error on 10 runs obtained by the time-adaptive approach in [4] was $8.0\% \pm 0.56\%$. Neither the baseline PINN nor the nonadaptive weighted scheme, with initial condition weight $C = 100$, were able to solve this PDE satisfactorily, with L2 errors $96.15\% \pm 6.45\%$ and $49.61\% \pm 2.50\%$, respectively (these numbers matched almost exactly those reported in [4]).

Figure 2 is unique to the proposed self-adaptive PINN algorithm. It displays the trained weights for the collocation points across the spatio-temporal domain. These are the weights of the multiplicative soft attention mask self-imposed by the PINN. This plot stays remarkably constant across different runs with random restarts, which is an indication that it is a property of the particular PDE being solved. We can observe that in this case, more attention is needed early in the solution, but not uniformly across the space variable. In [4], this observation was justified by the fact that the Allen-Cahn PDEs describes a time-irreversible diffusion-reaction processes, where the solution has to be approximated well early. However, here this fact is “discovered” by the self-adaptive PINN itself.

5 Conclusion

In this paper, we introduced Self-Adaptive Physically-Informed Neural Networks, a novel class of physically-constrained neural networks. This approach uses a similar conceptual framework as soft self-attention mechanisms used in Computer Vision, in that the network identifies which inputs are most important to its own training. It was shown that training of the Self-Adaptive PINN is formally equivalent to solving a PDE-constrained optimization problem using penalty-based method, though in a way where the monotonically-nondecreasing penalty coefficients are trainable. Experimental results with Burgers’, Helmholtz, and Allen-Cahn PDEs indicate that Self-Adaptive PINNs allow generate more accurate solutions of PDEs with smaller computational cost than other state-of-the-art PINN algorithms.

We believe that self-adaptive PINNs open up new possibilities for the use of deep neural networks in forward and inverse modeling in engineering and science. However, there is much that is not known yet about this class of algorithms, and indeed PINNs in general. For example, the use of standard

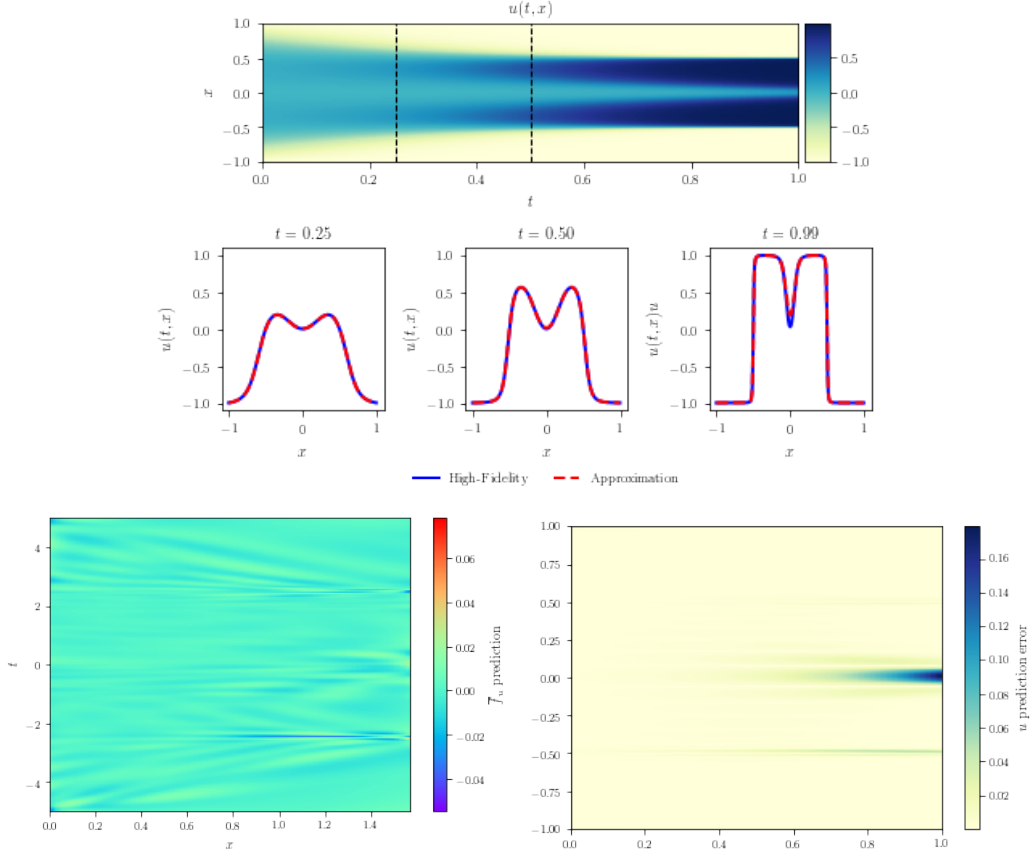


Figure 1: *Top*: Plot of the approximation $u(x, t)$ via the self-adaptive PINN. *Middle*: Snapshots of the approximation $u(x, t)$ vs. the high-fidelity solution $U(x, t)$ at various time points through the temporal evolution. *Bottom left*: Residual $r(x, t)$ across the spatial-temporal domain. As expected, it is close to 0 for the whole domain Ω . *Bottom right*: Absolute error between approximation and high-fidelity solution across the spatial-temporal domain.

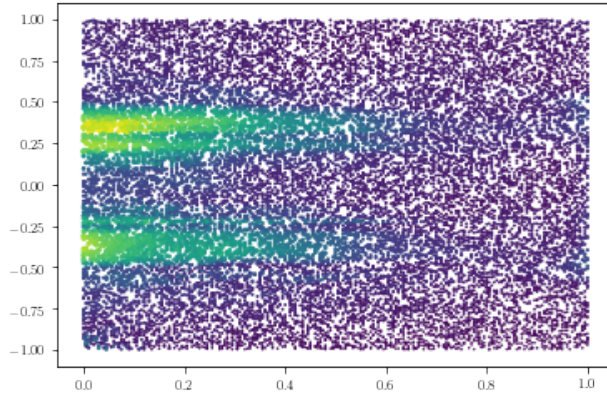


Figure 2: Learned weights across the spatio-temporal domain. Brighter colors and larger points indicate larger weights.

off-the-shelf optimization algorithms for training deep neural networks, such as Adam, may not be appropriate, since those algorithms were mostly developed for image classification problems. How to obtain optimization algorithms specifically tailored to PINN problems in an open problem. In addition, the relationship between PINNs and constrained-optimization problems, hinted at here, is likely a profound and fruitful topic of future study.

Acknowledgments

The authors would like to acknowledge the support of the D³EM program funded through NSF Award DGE-1545403. The authors would further like to thank the US Army CCDC Army Research Lab for their generous support and affiliation.

Appendix

Here we present additional experimental results with Burgher's and Helmholtz PDEs, which confirmed the trends observed previously.

Burgers' Equation

The viscous Burgers' PDE considered here is

$$u_t + uu_x - (0.01/\pi)u_{xx} = 0 \quad (34)$$

$$u(0, x) = -\sin(\pi x) \quad (35)$$

$$u(t, -1) = u(t, 1) = 0 \quad (36)$$

where $x \in [-1, 1]$ and $t \in [0, 1]$

All results for Burgers equation were generated from a fully-connected network with input layer size 2 corresponding to inputs of (x, t) , 8 hidden layers of 20 neurons each, and an output layer of size 1 corresponding to the output of the approximation $u(x, t)$. This directly mimics the setup of the results presented in [2]. All training is done for 10k iterations of Adam, followed by 10k iterations of L-BFGS to fine tune the network weights, consistent with related work. Additionally, the number of points selected for the trials shown are $N_0 = 100$, $N_b = 200$, and $N_r = 10000$. Training with this architecture took 96ms/iteration on a single Nvidia V100 GPU.

We achieved an L2 error of $4.803e-04 \pm 1.01e-4$ over 10 random restarts, which is a smaller error than the errors reported in [2] in 1/5 of the number of training iterations for an identical fully-connected architecture. The high-fidelity and predicted solutions are displayed in figure 3. Figure 4 demonstrate the accuracy of the proposed approach, using a significantly shorter training horizon than the baseline PINN.

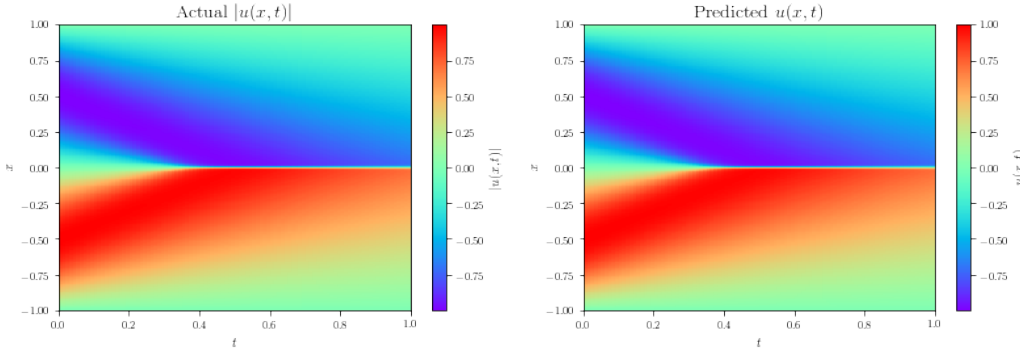


Figure 3: High-fidelity (left) vs. predicted (right) solutions for Burgers' equation

Figure 5 shows that the sharp discontinuity at $x = 0$ in the solution has correspondingly large weights, indicating that the model must pay extra attention to those particular points in its solution, resulting in an increase in approximation accuracy and training efficiency.

Helmholtz Equation

The Helmholtz equation model is typically used to describe the behavior of wave and diffusion processes, and can be employed to model evolution in a spatial domain or combined spatial-temporal

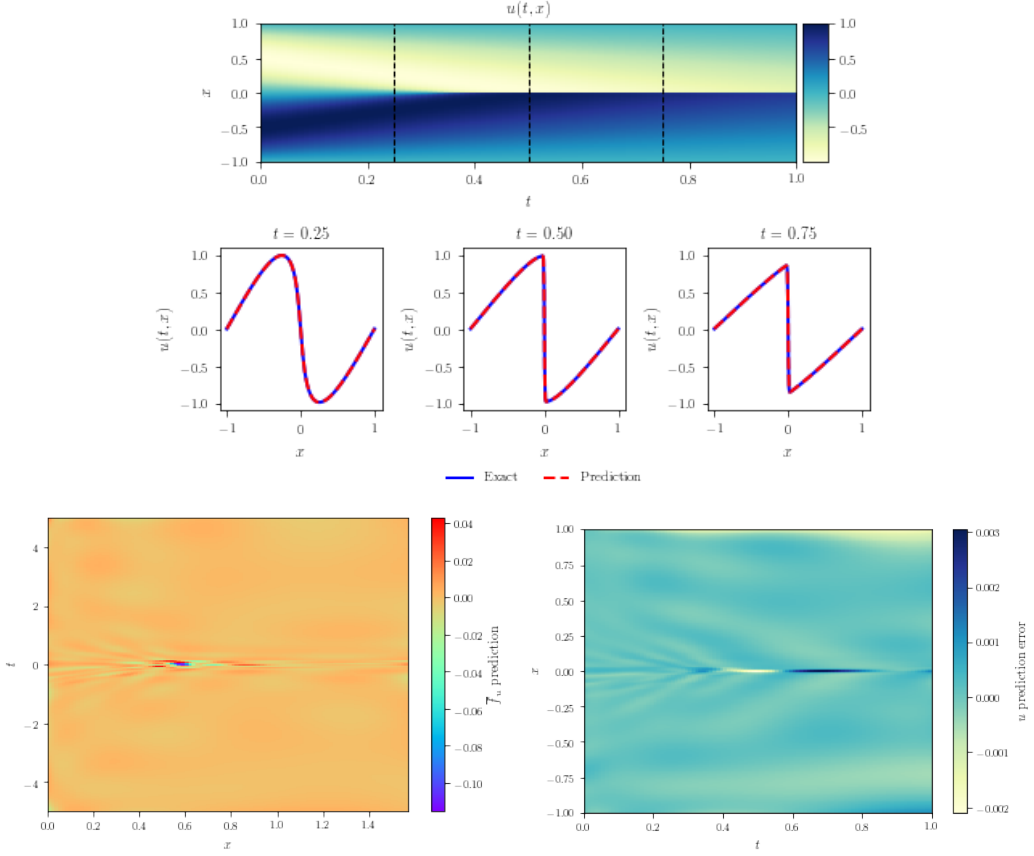


Figure 4: *Top*: predicted solution of Burger’s equation. *Middle*: Cross-sections of the approximated vs. actual solutions for various x-domain snapshots. *Bottom left*: Residual $r_u(x, t)$ across the spatial-temporal domain. *Bottom right*: Absolute error between prediction and high-fidelity solution across the spatial-temporal domain.

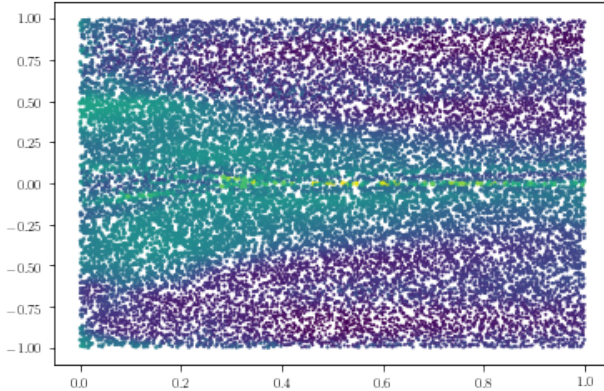


Figure 5: Trained weights for collocation points across the domain Ω . Larger/brighter colored points correspond to larger weights.

domain. Here we study a particular Helmholtz PDE existing only in the spatial (x, y) domain, described as:

$$u_{xx} + u_{yy} + k^2 u - q(x, y) = 0 \quad (37)$$

$$u(-1, y) = u(1, y) = u(x, -1) = u(x, 1) = 0 \quad (38)$$

where $x \in [-1, 1]$, $y \in [-1, 1]$ and

$$\begin{aligned} q(x, y) = & - (a_1 \pi)^2 \sin(a_1 \pi x) \sin(a_2 \pi y) \\ & - (a_2 \pi)^2 \sin(a_1 \pi x) \sin(a_2 \pi y) \\ & + k^2 \sin(a_1 \pi x) \sin(a_2 \pi y) w \end{aligned} \quad (39)$$

is a forcing term that results in a closed-form analytical solution

$$u(x, y) = \sin(a_1 \pi x) \sin(a_2 \pi y). \quad (40)$$

To allow a direct comparison to the results reported in [12], we take $a_1 = 1$ and $a_2 = 4$ and use the same neural network architecture with layer sizes [2, 50, 50, 50, 50, 1]. Our architecture is trained for 10k Adam and 10k L-BFGS iterations, again keeping the self-adaptive mask weights constant through the L-BFGS training iterations and only allowing those to train via Adam. We sample $N_b = 400$ (100 points per boundary). Given the steady-state initialization and constant forcing term, there is no applicable initial condition and consequently no N_0 . We create a mesh of size (1001,1001) corresponding to the $x \in [-1, 1]$, $y \in [-1, 1]$ range, yielding 1,002,001 total mesh points, from which we select $N_r=100$ k residual collocation points.

We can see in figure 6 that the Self-Adaptive PINN prediction is very accurate and indistinguishable from the exact solution. We achieve a relative L2 error of $3.2\text{e-}3 \pm 2.2\text{e-}4$, which improves upon the learning-rate annealing weighted scheme proposed in [12], and begins to encroach on the accuracy of their improved fully-connected scheme with no additional modifications to the network structure itself. It is also worth noting that the Self-Adaptive PINN is trained for 1/2 of the training iterations listed in [12] as well (at 10k Adam and 10 L-BFGS vs. 40k Adam), and achieves better L2 accuracy than a comparable architecture listed in table 2 of [12].

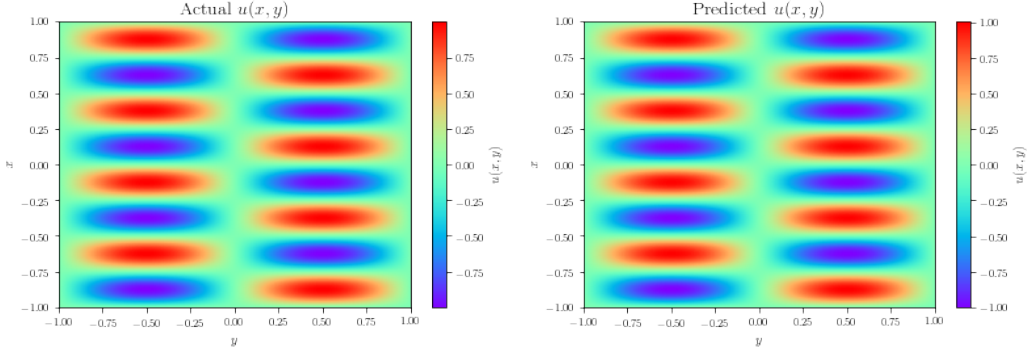


Figure 6: Exact (*left*) vs. predicted (*right*) solutions for Helmholtz equation

Figure 7 shows individual cross-sections of the Helmholtz solution, demonstrating the Self-Adaptive PINN's ability to accurately approximate the sinusoidal solution on the whole domain. Figure 8 shows that the Self-Adaptive PINN largely ignores the flat areas in the solution, while focusing its attention on the nonflat areas.

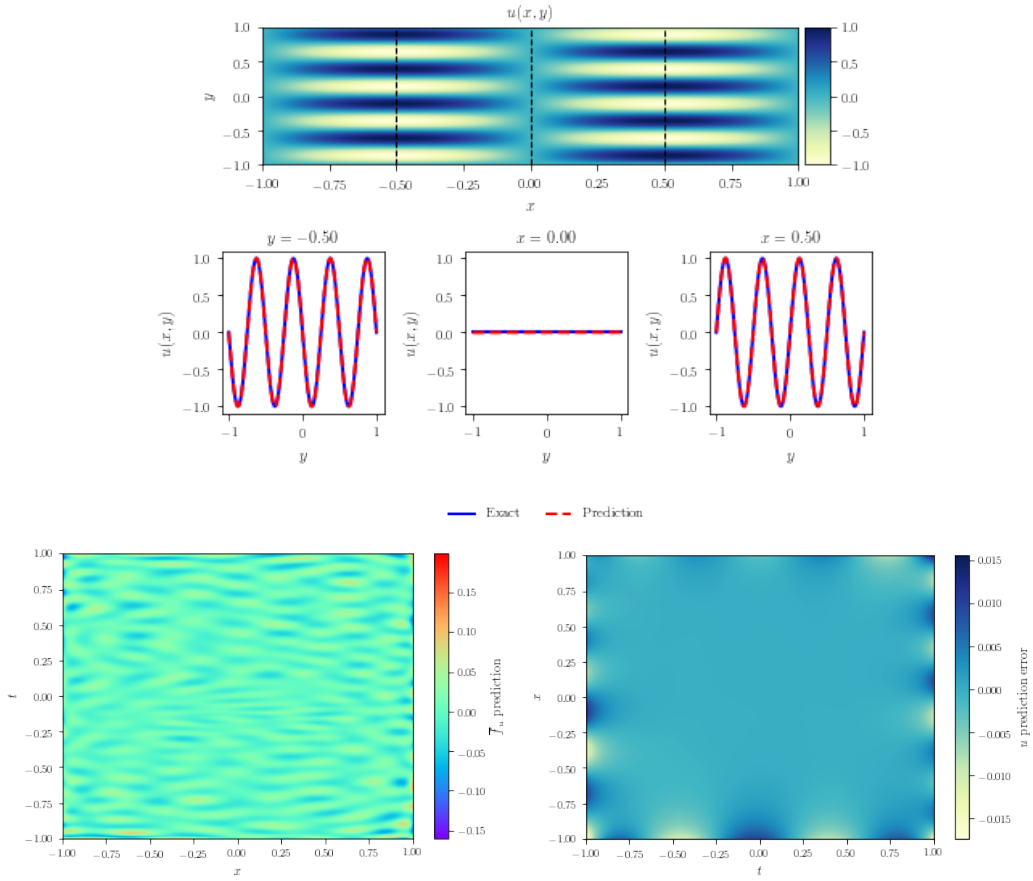


Figure 7: *Top* predicted solution of Helmholtz equation. *Bottom* Cross-sections of the approximated vs. actual solutions for various x-domain snapshots

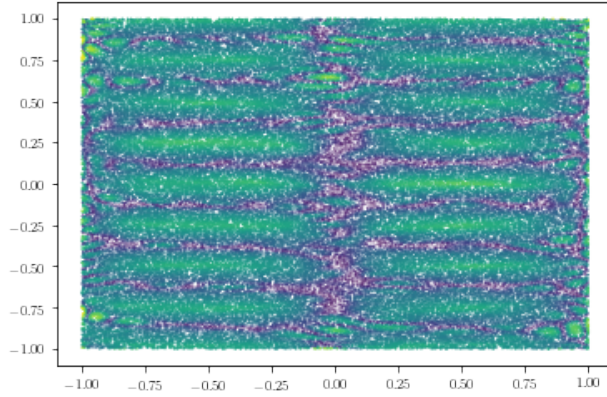


Figure 8: Self-learned weights after training via Adam for the Helmholtz system. Brighter/larger points correspond to larger weights.

References

- [1] Nathan Baker, Frank Alexander, Timo Bremer, Aric Hagberg, Yannis Kevrekidis, Habib Najm, Manish Parashar, Abani Patra, James Sethian, Stefan Wild, Karen Willcox, and Steven Lee. Workshop report on basic research needs for scientific machine learning: Core technologies for artificial intelligence, 2 2019.
- [2] Maziar Raissi, Paris Perdikaris, and George E Karniadakis. Physics-informed neural networks:

A deep learning framework for solving forward and inverse problems involving nonlinear partial differential equations. *Journal of Computational Physics*, 378:686–707, 2019.

- [3] Maziar Raissi. Forward-backward stochastic neural networks: Deep learning of high-dimensional partial differential equations. *arXiv preprint arXiv:1804.07010*, 2018.
- [4] Colby L Wight and Jia Zhao. Solving allen-cahn and cahn-hilliard equations using the adaptive physics informed neural networks. *arXiv preprint arXiv:2007.04542*, 2020.
- [5] Sifan Wang, Xinling Yu, and Paris Perdikaris. When and why pinns fail to train: A neural tangent kernel perspective. *arXiv preprint arXiv:2007.14527*, 2020.
- [6] MWMG Dissanayake and N Phan-Thien. Neural-network-based approximations for solving partial differential equations. *communications in Numerical Methods in Engineering*, 10(3):195–201, 1994.
- [7] Martín Abadi, Paul Barham, Jianmin Chen, Zhifeng Chen, Andy Davis, Jeffrey Dean, Matthieu Devin, Sanjay Ghemawat, Geoffrey Irving, Michael Isard, et al. Tensorflow: A system for large-scale machine learning. In *12th {USENIX} symposium on operating systems design and implementation ({OSDI} 16)*, pages 265–283, 2016.
- [8] Jarrett Revels, Miles Lubin, and Theodore Papamarkou. Forward-mode automatic differentiation in julia. *arXiv preprint arXiv:1607.07892*, 2016.
- [9] Atilim Güneş Baydin, Barak A Pearlmutter, Alexey Andreyevich Radul, and Jeffrey Mark Siskind. Automatic differentiation in machine learning: a survey. *The Journal of Machine Learning Research*, 18(1):5595–5637, 2017.
- [10] Adam Paszke, Sam Gross, Soumith Chintala, Gregory Chanan, Edward Yang, Zachary DeVito, Zeming Lin, Alban Desmaison, Luca Antiga, and Adam Lerer. Automatic differentiation in pytorch. 2017.
- [11] Richard L Burden and Douglas J Faires. Numerical analysis. 1985.
- [12] Sifan Wang, Yujun Teng, and Paris Perdikaris. Understanding and mitigating gradient pathologies in physics-informed neural networks. *arXiv preprint arXiv:2001.04536*, 2020.
- [13] Nele Moelans, Bart Blanpain, and Patrick Wollants. An introduction to phase-field modeling of microstructure evolution. *Calphad*, 32(2):268–294, 2008.
- [14] Fei Wang, Mengqing Jiang, Chen Qian, Shuo Yang, Cheng Li, Honggang Zhang, Xiaogang Wang, and Xiaou Tang. Residual attention network for image classification. In *Proceedings of the IEEE conference on computer vision and pattern recognition*, pages 3156–3164, 2017.
- [15] Yanwei Pang, Jin Xie, Muhammad Haris Khan, Rao Muhammad Anwer, Fahad Shahbaz Khan, and Ling Shao. Mask-guided attention network for occluded pedestrian detection. In *Proceedings of the IEEE International Conference on Computer Vision*, pages 4967–4975, 2019.
- [16] Yi Zhou, Junjie Yang, Huishuai Zhang, Yingbin Liang, and Vahid Tarokh. Sgd converges to global minimum in deep learning via star-convex path. *arXiv preprint arXiv:1901.00451*, 2019.
- [17] David G Luenberger and Yinyu Ye. *Linear and nonlinear programming*. Springer, 3rd edition, 2008.
- [18] Walter E Lillo, Mei Heng Loh, Stefen Hui, and Stanislaw H Zak. On solving constrained optimization problems with neural networks: A penalty method approach. *IEEE Transactions on neural networks*, 4(6):931–940, 1993.
- [19] Valeri M Mladenov and N Maratos. Neural networks for solving constrained optimization problems. *Proc. of CSCC'00, Athens, Greece,(N. Mastorakis*, 2000.
- [20] Diederik P Kingma and Jimmy Ba. Adam: A method for stochastic optimization. *arXiv preprint arXiv:1412.6980*, 2014.
- [21] Dong C Liu and Jorge Nocedal. On the limited memory bfgs method for large scale optimization. *Mathematical programming*, 45(1-3):503–528, 1989.
- [22] Jie Shen and Xiaofeng Yang. Numerical approximations of allen-cahn and cahn-hilliard equations. *Discrete & Continuous Dynamical Systems-A*, 28(4):1669, 2010.
- [23] Courtney Kunselman, Vahid Attari, Levi McCleeny, Ulisses Braga-Neto, and Raymundo Arroyave. Semi-supervised learning approaches to class assignment in ambiguous microstructures. *Acta Materialia*, 188:49–62, 2020.